

Numerical model for nonlinear analysis of composite concrete-steel-masonry bridges

Goran Baloevic^{*}, Jure Radnic^a, Nikola Grgic^b, Domagoj Matesan^c and Marija Smilovic^d

*Faculty of Civil Engineering, Architecture and Geodesy, University of Split,
Matice hrvatske 15, 21 000 Split, Republic of Croatia*

(Received July 16, 2015, Revised January 21, 2016, Accepted February 16, 2016)

Abstract. This paper firstly briefly describes developed numerical model for both static and dynamic analysis of planar structures made of concrete, steel and masonry. The model can simulate the main nonlinearity of such individual and composite structures. The model is quite simple and based on a small number of material parameters. After that, three real composite concrete-steel-masonry bridges were analyzed using the presented numerical model. It was concluded that the model can be useful in practical analysis of composite bridges. However, future verifications of the presented numerical model are desirable.

Keywords: numerical model; concrete-steel-masonry composite bridges; static and dynamic analysis

1. Introduction

Unreinforced and reinforced concrete, steel and masonry are the most widely used building materials for bridges. Herein, some bridges are constructed from a single material and some from combination of these materials. In reliable static and dynamic analysis of bridges constructed from different materials, it is necessary to use such material models that can simulate main nonlinear effects of individual material. Adequate simulation of the behavior on the contact surface between individual materials is also necessary.

So far, a great number of numerical models for static and dynamic analysis of bridges and structures have been developed. Herein, a significant difference exists regarding precision and reliability of these models. Some of them can be found hereinafter.

Yang and Yau (1997) developed an interaction element that is both accurate and efficient for modeling the vehicle bridge interaction of railway bridges carrying high-speed trains. Brownjohn and Xia (2000) investigated the application of sensitivity-based model updating technology to the dynamic assessment of the Safti Link Bridge, a curved cable-stayed bridge in Singapore. Cunha *et*

*Corresponding author, Ph.D., E-mail: goran.baloevic@gradst.hr

^a Professor, E-mail: jure.radnic@gradst.hr

^b Ph.D., E-mail: nikola.grgic@gradst.hr

^c Professor, E-mail: domagoj.matesan@gradst.hr

^d Ph.D., E-mail: marija.smilovic@gradst.hr

al. (2001) described the dynamic tests performed on a large cable-stayed Vasco da Gama bridge, and used the 3D numerical finite-element model to compare the obtained dynamic properties. Song *et al.* (2003) and presented a new three-dimensional finite element analysis model of high-speed train-bridge interactions. Chung and Sotelino (2006) developed a three-dimensional finite element modeling of composite girder bridges. Abdessemed *et al.* (2011) performed both experimental and numerical dynamic analysis of a bridge repaired by CFRP. Berchio *et al.* (2016) modeled the roadway of a suspension bridge as a thin rectangular plate and studied in detail its oscillating modes. Fu (2016) presented a numerical solution for the dynamic response of a simply supported bridge with a switching crack subjected to seismic excitations and moving trains. Wang *et al.* (2016) proposed a new approach for determining the reasonable number of stress cycles for the fatigue design of simply-supported steel I-girder bridges which takes the dynamic effect of vehicle loading into account. Li *et al.* (2016) investigated the dynamic property of a specially shaped hybrid girder bridge with concrete-filled steel tube (CSFT) arches based on experimental and numerical methods, especially under moving vehicles.

The purpose of this paper is a presentation of developed numerical model for nonlinear static and dynamic analysis of planar structures made of concrete, steel and masonry, and illustration of its application in analysis of some composed bridges in practice. Analyzed structures can be made from a single material or from combination of above-mentioned materials (composite structures). The soil model is also included for the modelling of soil-structure coupled problems. In order to promote wide practical application, the developed numerical model is quite simple and is based on a small number of material parameters. The model can simulate main nonlinear effects of individual material, nonlinear behavior on the contact surface between different materials, changes in the system geometry (geometric nonlinearity) and different phases of construction. Loading can only be applied in the plane of the structure. Lateral structural stability is not included in the model.

By applying the presented numerical model, three real composite bridges made of several building materials were analyzed. Solved examples illustrate some possibilities of the presented numerical model for static and dynamic (seismic) analysis of composite bridges.

2. A brief description of the developed numerical model

2.1 General

The presented numerical model represents the integration and upgrade of previously developed numerical models for static and dynamic analysis of individual planar structures made of concrete, steel and masonry (Radnic *et al.* 2011, 2013 and Baloevic *et al.* 2013). Particular, the described model combines previously developed models (software) for the analysis of individual structures made of concrete, steel or masonry into a single model (software) for the analysis of composite concrete-steel-masonry structures. To simulate any possible nonlinearity at the contact surfaces, contact elements with appropriate nonlinear normal stress-normal strain and shear stress-normal stress relationships are included. The model is also upgraded with simulation of the construction of a structure in different phases. Main properties of the model are given hereinafter. The finite element method is used for the spatial discretization of the analysed problem. Finite difference method is adopted for the time discretization of the dynamic equation of motion. The implicit or the implicit-explicit Newmark's time algorithms can be used, developed in iterative form by

Hughes *et al.* (1979). Basic eight-node serendipity finite elements are used. There are adopted 6-node planar and 2-node bar elements for contact elements. To include the effects of large displacements, updated Lagrange formulation can be used. The formation of a structure over different phases is simulated by memorizing the current state of displacements, strains, stresses and damages, and successively forming a new spatial discretization of the structure. Convergence criterion of incremental-iterative procedure is given as a function of current displacements increment in relation to total displacements. The adopted constitutive models for reinforced concrete (concrete and reinforcing steel), structural steel, masonry, soil and contact elements are briefly presented only.

2.2 Material models

2.2.1 Reinforced concrete model

Graphical presentation of the constitutive model for concrete is given in Fig. 1. The theory of plasticity is used for concrete behaviour in compression, with defined yield criterion, flow rule and crushing criterion (see Fig. 1(a)). It is assumed that concrete is homogeneous and isotropic under low stress levels, with linear elastic stress-strain relation. After the yield criterion has been reached, an ideally plastic behaviour is adopted. The concrete crushing criterion is defined as a function of strain components. When the crushing criterion is achieved, it is assumed that the concrete has no stiffness. The cracks in concrete are modelled as smeared, neglecting the displacement discontinuity after concrete cracking. After crack opening, it is assumed that its position remains unchanged for the next loading and unloading. After that, the concrete becomes anisotropic and the crack direction determines the main directions of concrete anisotropy. Partial or full closing of previously opened cracks is modelled, as well as reopening of previously closed cracks. The transfer of compressive stress across a fully closed crack is modelled as for non-cracked concrete. After crack reopening, tensile stiffness of cracked concrete is not considered anymore.

The effects of tensile stiffness of cracked concrete is simulated by gradual decrease of tensile stress components perpendicular to the crack plane, in accordance with the adopted stress-strain relationship for uniaxial stress state (see Fig. 1(b)). Shear elasticity modulus of cracked concrete is reduced linearly, depending on the value of tensile concrete strain perpendicular to the crack plane (see Fig. 1(c)).

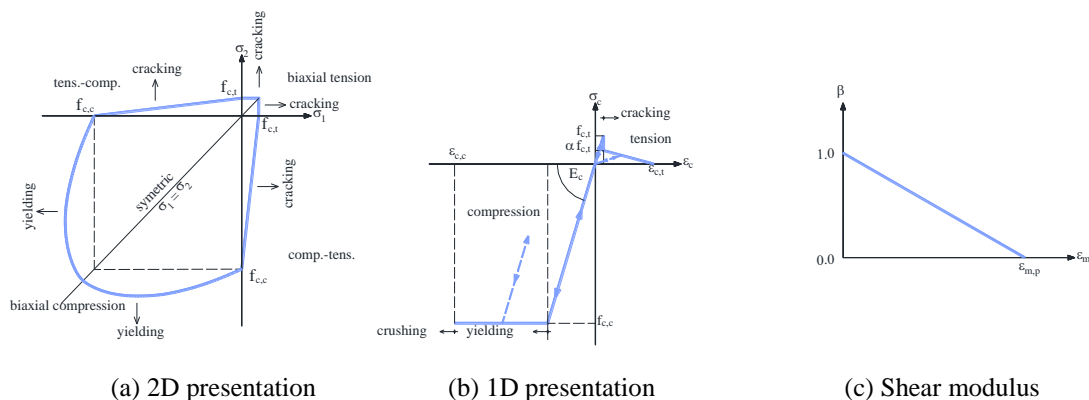


Fig. 1 Graphical illustration of the concrete model

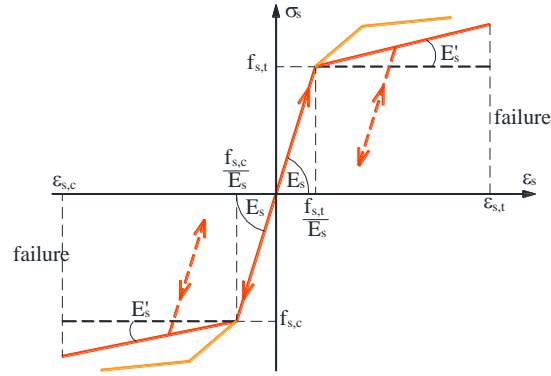
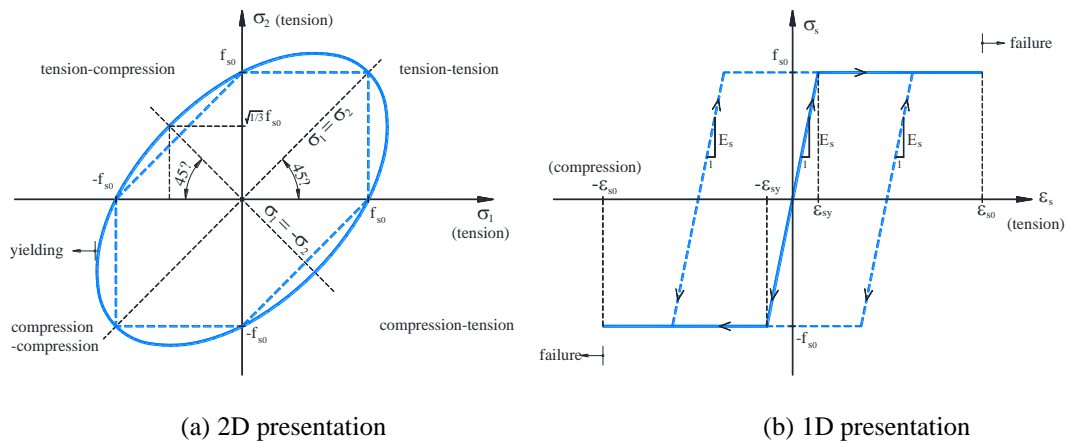


Fig. 2 Graphical illustration of the reinforcement model



(a) 2D presentation

(b) 1D presentation

Fig. 3 Graphical illustration of the structural steel model

Reinforcement (classical, cables, FRP) is simulated by bar element within basic concrete element. Arbitrary polygonal stress-strain relationship for bar material can be used (see Fig. 2). It is assumed that there is no slipping between concrete and reinforcement.

2.2.2 Steel model

Biaxial failure of planar steel structures is modelled by the effect of normal stresses only. A classical elasto-plastic model for structural steel is used, with linear behaviour in unloading (see Fig. 3). Same behaviour of steel in tension and compression is adopted. Von Mises yield criterion is used for steel yielding. The failure criterion of steel is defined as a function of principal strains, in an analogous way as a steel yielding.

2.2.3 Masonry model

Macro and micro model of masonry can be used. In the macro model, masonry is approximated

by a representative material whose physical-mechanical properties adequately describe the actual complex masonry properties. Such approach allows appliance of larger finite elements, significantly reduces the number of variables and rapidly accelerates the structural analysis. In the micro model, the spatial discretization can be performed at the level of unit elements, joint (mortar) and contact surface between them. It is possible to use various micro models of masonry. In relation to the masonry macro model, the masonry micro model can provide more accurately description of damage and failure of the masonry, but with much more complex analysis. This model is not convenient for practical analysis of most structures. A brief description of adopted masonry macro model is given below.

Adopted masonry macro model is similar to adopted concrete model described in section 2.2.1., with some differences. Masonry is treated as an orthotropic material, with orthotropic axes that coincide to bed and vertical joints (see Fig. 4). In that directions masonry has different material properties. There are two models of crack opening. In one model, cracks can be opened only in directions of joints. In the second model, cracks are perpendicular to the principal tensile stresses. In addition to the failure criterion of masonry in function of principal normal stresses, failure criterions in function of shear stress and corresponding normal stress are adopted.

2.2.4 Soil model

A special constitutive soil model has not been developed. Only the concrete model described in section 2.2.1., or masonry model described in section 2.2.3., can be used. However, a homogeneous isotropic soil can be adequately simulated using the concrete material model, where model’s parameters (uniaxial strengths and strains, modulus of elasticity, etc.) have to represent soil properties properly. Also, an anisotropic soil with different properties in horizontal and vertical direction can be adequately simulated using the orthotropic masonry model, with proper definition of soil parameters in both horizontal and vertical direction.

2.2.5 Material model of contact elements

2D contact elements transmit normal stress through the contact surface according to selected stress-strain relation (see Fig. 5). In this way, penetration and separation on the contact surface between different materials can be simulated.

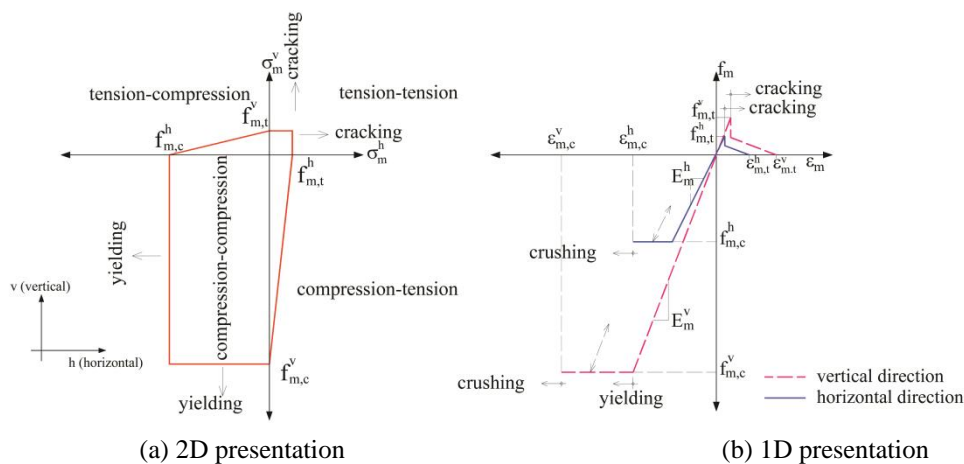


Fig. 4 Graphical illustration of the masonry model

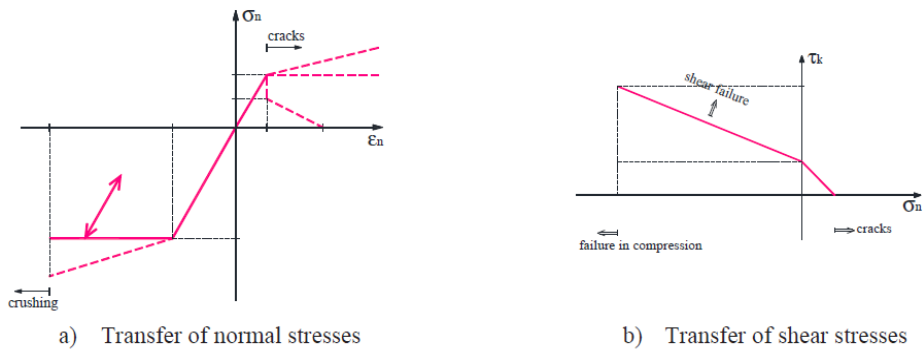


Fig. 5 Graphical illustration of the material model for contact elements

This contact element can also transmit shear stress along the contact surface, in a function of normal stress perpendicular to this surface, that can simulate the sliding along it. 1D contact element simulates a bar that passes through the 2D contact element, and can model the transfer of normal and shear stress according to the selected normal stress - normal strain and shear stress - normal stress diagrams.

3. Analysed examples

To illustrate some possible applications of the presented numerical model and developed computational program 2D-COMPS, static and dynamic analyses of three real composite concrete-steel-masonry bridges were performed. Only some obtained results are given hereinafter.

3.1 Old stone bridge in Mostar

The Old Stone Bridge in Mostar in Bosnia and Herzegovina (see Fig. 6), across the turbulent and unpredictable Neretva River, was constructed in 1566. The bridge architect was Hayruddin, a co-worker of a famous Ottoman architect Koca Mimar Sinan, and it is accepted as one of the most beautiful stone bridges in the world. The bridge is on the UNESCO world heritage list of the highest category. The bridge has an extremely slender stone arch, of span about 30 m and thickness of 0.8 m (see Fig. 7). The arch width is 3.95 m. It has 111 rows of 0.4 m wide stone blocks. The stone blocks are interconnected by metal cramps and wedges. The bridge was destroyed in 1993, during the recent war in Bosnia and Herzegovina. The bridge and surrounding towers were completely reconstructed in 2004 in accordance with the authentic state, with the support of the European Community. The cracks were observed in the stone arch in several places in November 2007.

Detailed analysis of the considered problem can be found in Radnic *et al.* (2012). For spatial discretization of the bridge, two planar models were considered: NM1 – where the bridge was simulated by arch only, with very refined spatial discretization, and NM2 – where the spatial model consists of the arch, upper arch assembly and abutments. The effects of static vertical

loadings, temperature changes (see Fig. 8; Mostar has very high temperatures in the summer) and accelerogram of the earthquake Ston, with epicentre in Ston (Croatia) about 55 km southeast from Mostar, on the bridge response were investigated. Horizontal component of the accelerogram of the earthquake Ston is shown in Fig. 9. Vertical component of the accelerogram was created by scaling the horizontal accelerogram with the factor of 0.75.

Only some results of the analysis of the model NM2 are shown. Contact elements are used at the accepted boundaries of the spatial model. Horizontal displacements are restricted at the lateral edges of the model, as well as both vertical and horizontal displacements at the contact with the soil. The calculated first period of free oscillations of the bridge (see Fig. 10) is $T_1 = 0.086$ s (longitudinal mode vibration) and the second period is $T_2 = 0.072$ s (vertical mode vibration), which agree well with the corresponding measured values of $T_1 = 0.087$ s and $T_2 = 0.071$ s (Krstevska *et al.* 2008). For the dead loads, computational deflection of the arch in the apex is 0.94 mm (see Fig. 11), which almost coincides with the measured displacement after removing the scaffolds of 0.9 mm (south side).



Fig. 6 The old stone bridge in Mostar (before demolition)

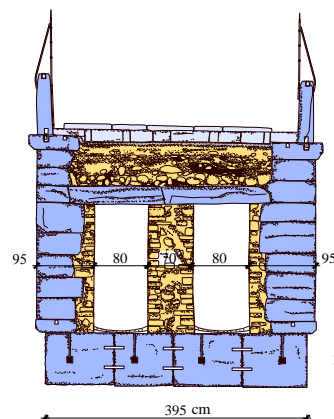


Fig. 7 The cross-section of the bridge

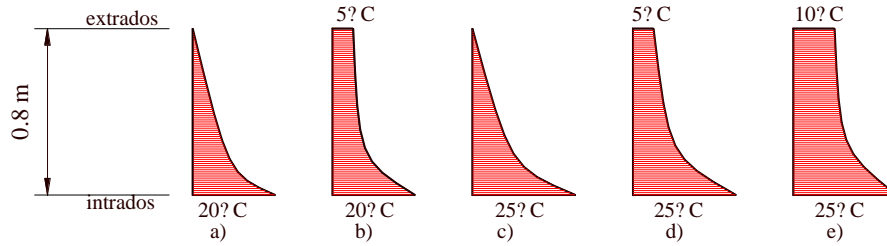


Fig. 8 Some considered temperature changes across the arch thickness

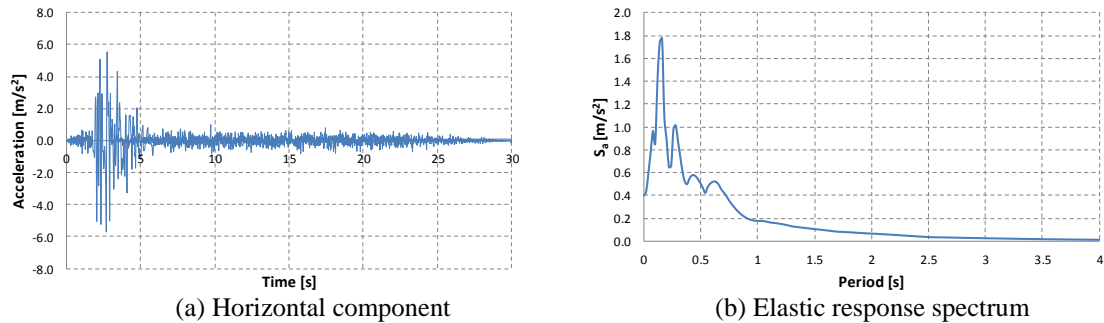


Fig. 9 Accelerogram of the earthquake Ston (1996)

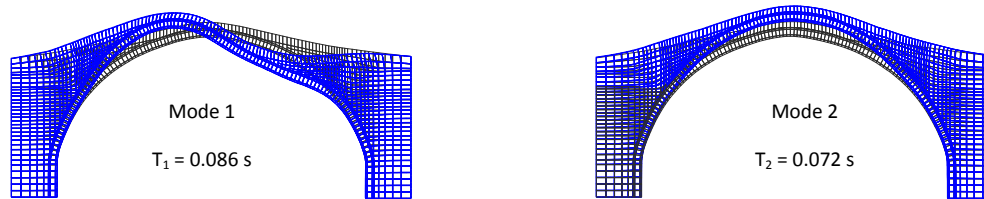


Fig. 10 First two modes of free vibrations of the bridge

Some results of the analysis for dead load and temperature changes according to Fig. 8(a) are shown in Fig. 12. The effect of temperature changes has proven as very unfavorable.

Deflections and cracking zones of the stone arch obtained by the performed analysis agrees well with that on real restored arch. The main cause of the damage to the original and the restored stone arch is inadequate quality of stone tenelija and above all its low tensile strength, as well as large temperature changes. Increased damage to the restored arch in the short time period probably is the consequence of deviations of some solutions from those of the original bridge. However, the restored arch is stronger than the original one, and the effect of temperature changes in more unfavorable. Stone block with somewhat lower strength than the original blocks were used, spaces are formed in the upper part of the abutment, etc.

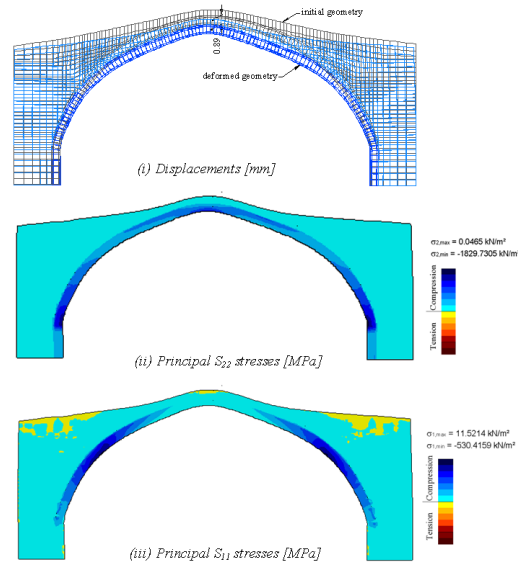


Fig. 11 Some numerical results for the model NM2 – dead loads

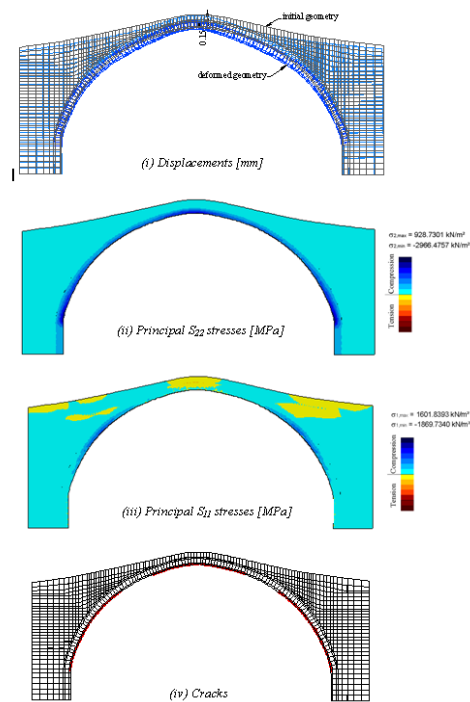
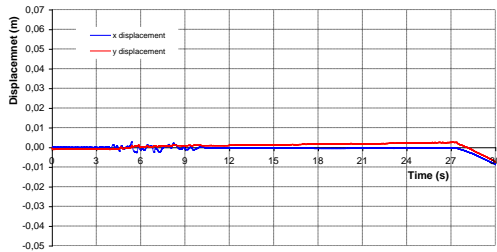
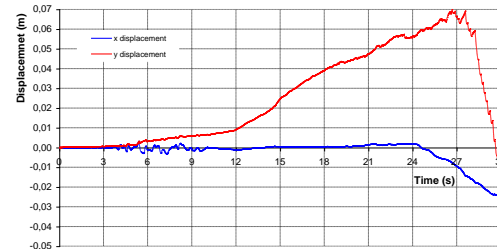


Fig. 12 Some numerical results for the model NM2 – dead load and temperature changes according to Fig. 8(a)

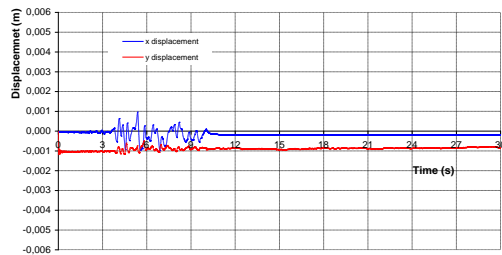


(a) Sustained load and earthquake

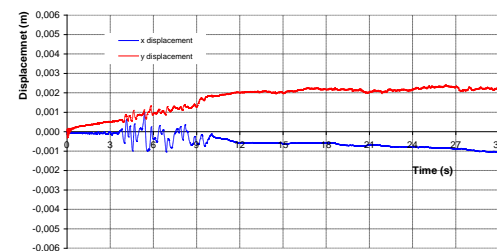


(b) Dead load, temperature changes according to Fig. 8(a) and earthquake

Fig. 13 Displacement in the arch apex for earthquake Ston



(a) Sustained load and earthquake



(b) Dead load, temperature changes according to Fig. 8(a) and earthquake

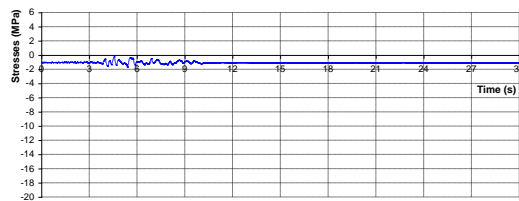
Fig. 14 Displacement in the arch apex for scaled earthquake Ston (PGA = 0.3 g)

Viscous damping was assumed to be 2% in the dynamic analyses, next to direct influence of nonlinearity through nonlinear material models.

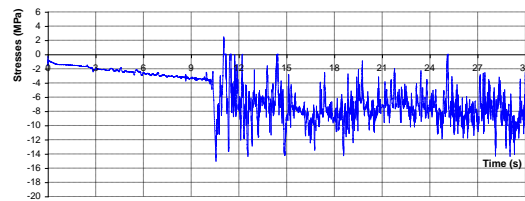
Displacement in the arch apex for earthquake Ston (low-probability for appearance of such strong earthquake at the location of the bridge) is shown in Fig. 13. Beside combination of the dead load and the earthquake (see Fig. 13(a)), the combination with the dead load, temperature changes and earthquake (see Fig. 13(b)) was also analyzed, due to possible high temperature changes during the earthquake action. In Fig. 13(b), the effect of temperature changes on the vertical displacement in the arch apex (deflection up of about 70 mm) is noticeable. The vertical displacement drops suddenly after $t = 27$ s, as a result of the effect of the dead load after progressive yielding of stone blocks and loss of strength in the arch.

Displacements for scaled earthquake Ston with peak ground acceleration $PGA = 0.3$ g are shown in Fig. 14 (maximal design acceleration for the area of Mostar). It is obvious that the displacements are smaller for the scaled earthquake Ston than for the real one.

For the scaled earthquake Ston, stress in the stone block in the arch heel near the intrados is shown in Fig. 15 and stress in the metal cramp in the arch apex near the intrados is shown in Fig. 16.

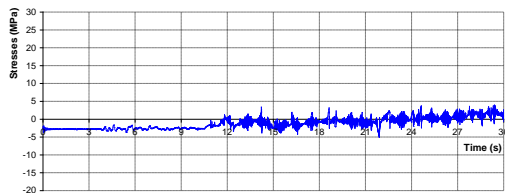


(a) Sustained load and earthquake

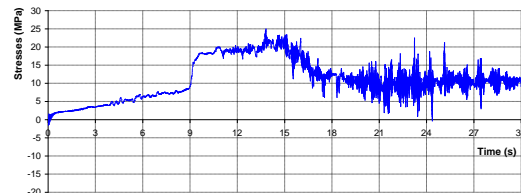


(b) Dead load, temperature changes according to Fig. 8(a) and earthquake

Fig. 15 Stress in stone block in arch heel near the intrados for scaled earthquake Ston (PGA = 0.3 g)



(a) Sustained load and earthquake



(b) Dead load, temperature changes according to Fig. 8(a) and earthquake

Fig. 16 Stress in metal cramp in arch apex near the intrados for scaled earthquake Ston (PGA = 0.3 g)

3.2 Concrete bridge across Cetina river

Concrete girder bridge across Cetina river near the town of Omis in Croatia (Figs.17 and 18) was analysed, as a part of its renovation project. However, to withstand traffic loads, concrete girders are strengthened with FRP thin tapes for taking over bending moments in the span and above supports, and with FRP sheets for taking over shear forces near supports. Strengthened bridge satisfies terms of bearing capacity and deformability according to existing Croatian norms HRN EN 1992-2:2013 and HRN EN 1998-2:2011. Both static and dynamic analyses for the original and strengthened bridge were performed. Scaled earthquake Ston with $PGA = 0.2$ g was used, which represents maximal design acceleration at the location of the bridge. In the spatial model of the bridge, abutments are omitted since the span structure is supported over horizontal free beds. At these points, vertical displacement of the structure is restricted. Contact elements are placed below foundation to simulate their rotation. In the dynamic analyses, viscous damping was assumed as 2%. FRP tapes and sheets are simulated as reinforcement, with the model shown in Fig. 2. Figs. 19-28 show only some results of the performed analyses.

Deflection in the first midspan of the bridge for gravitational and traffic load is shown in Fig. 19. The original bridge lost its stability with the traffic load factor of 1.45, while the strengthened bridge lost its stability with the factor of 2.0. The strengthened bridge showed greater stiffness compared to the original bridge.

Reinforcement stress in the first midspan for gravitational and traffic load is shown in Fig. 20.

For the equal traffic load, reinforcement stresses in the strengthened bridge are lower. Stress in FRP tape above the second support for gravitational and traffic load is shown in Fig. 21. At the ultimate bearing capacity of the bridge, a sudden increase of the stress in the FRP and failure at tensile strength of the tape occur.



Fig. 17 Concrete girder bridge across Cetina river

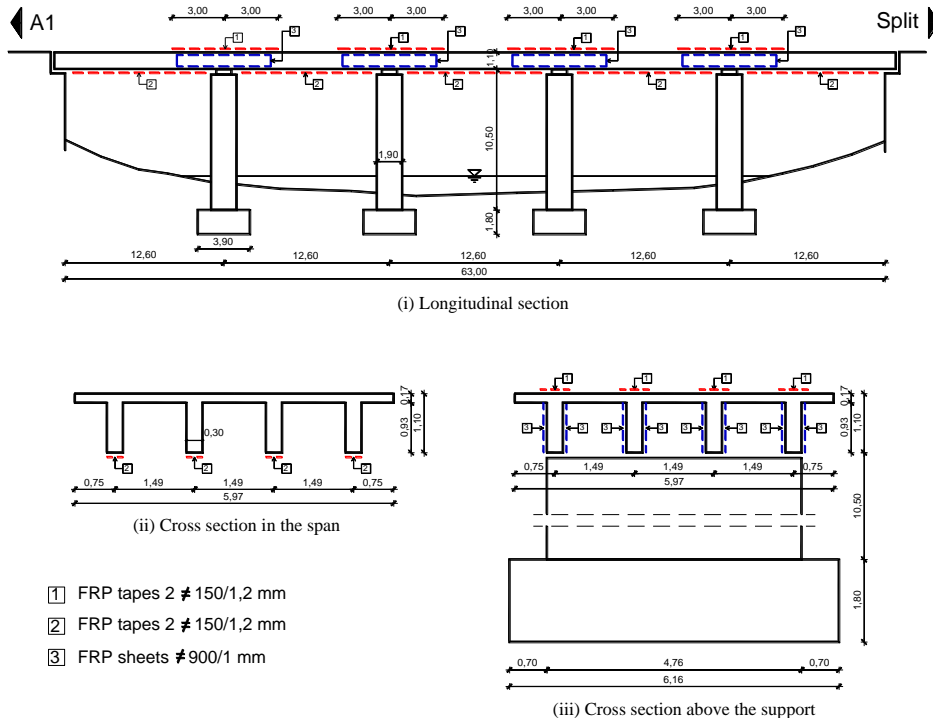


Fig. 18 Basic data of the analysed concrete girder bridge

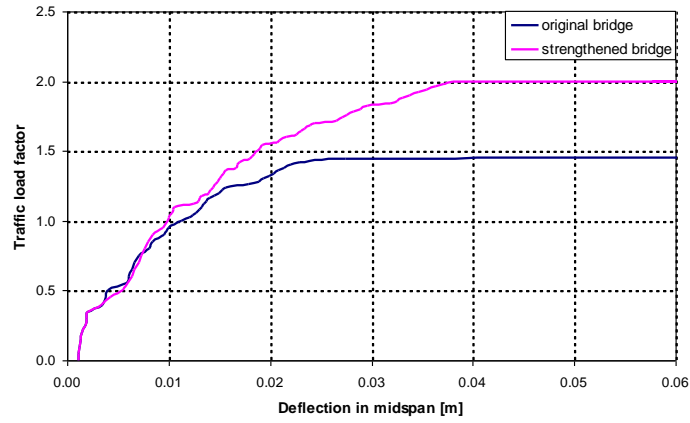


Fig. 19 Deflection in the first midspan of the bridge for gravitational and traffic loads

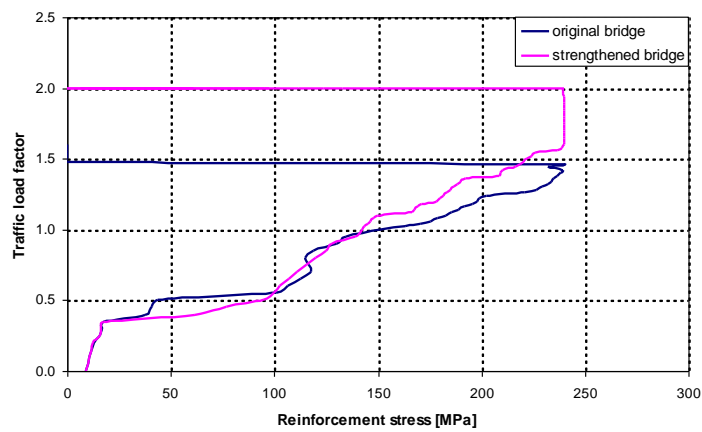


Fig. 20 Reinforcement stress in the first midspan for gravitational and traffic load

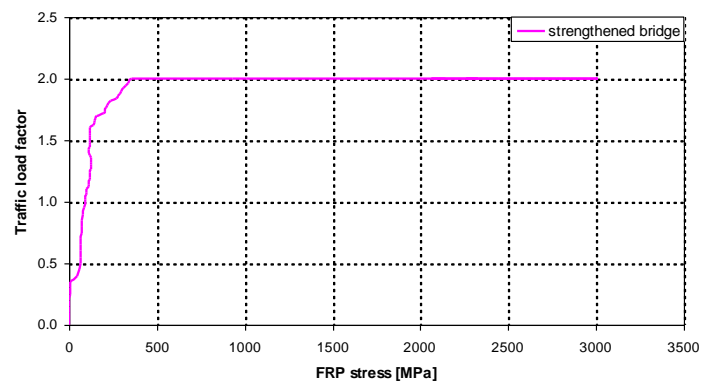


Fig. 21 Stress in FRP tape above the second support for gravitational and traffic load

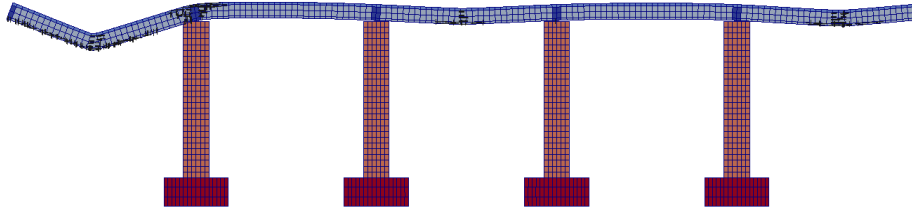


Fig. 22 Deformation and crack state of the strengthened bridge for gravitational and traffic load before failure

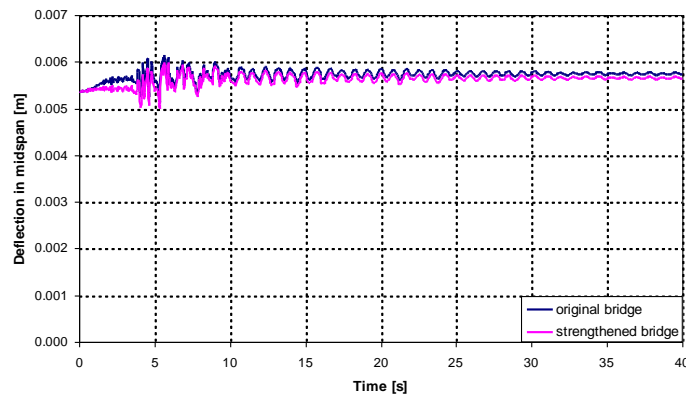


Fig. 23 Deflection in the first midspan of the bridge for scaled earthquake Ston

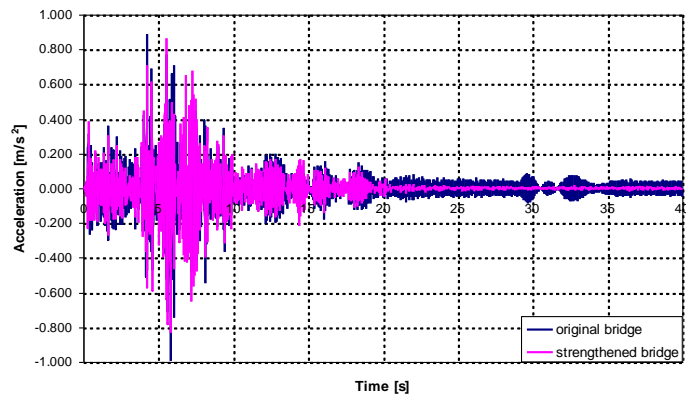


Fig. 24 Vertical acceleration in the first midspan of the bridge for scaled earthquake Ston

Deformation and crack state of the strengthened bridge for gravitational and traffic load before failure is shown in Fig. 22, where the adopted spatial discretization of the bridge can be noticed.

For the scaled earthquake Ston (in combination with the dead load and 50% of the traffic load), deflection in the first midspan is presented in Fig. 23, vertical acceleration in the first midspan in Fig.

24 and reinforcement stress in the first midspan in Fig. 25. It can be noticed that the stated variables are slightly different for the original bridge and the strengthened bridge.

Obtained results indicate that the strengthened bridge has greater bearing capacity and lower deflections compared to its previous state, in accordance with the requirements of Croatian norms HRN EN 1992-2:2013 and HRN EN 1998-2:2011.

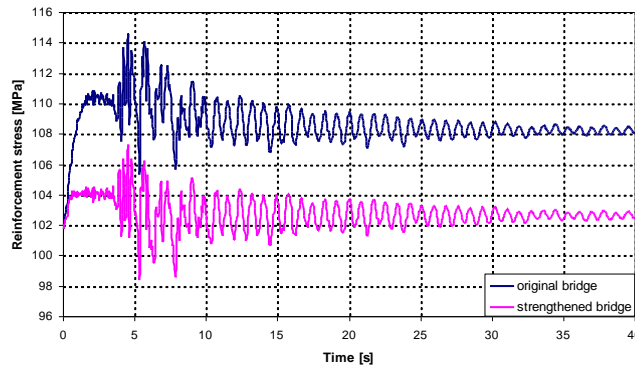


Fig. 25 Reinforcement stresses in the first midspan of the bridge for scaled earthquake Ston

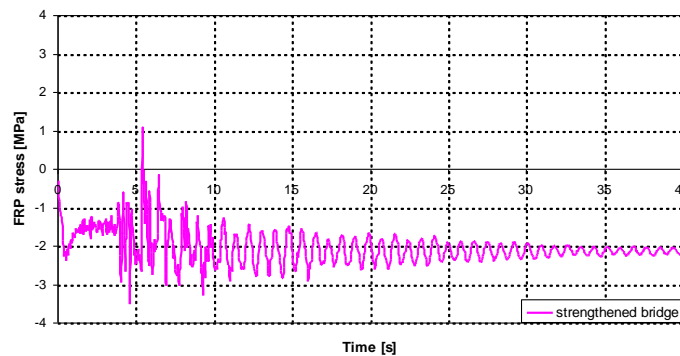


Fig. 26 FRP stresses in the first midspan of the bridge for scaled earthquake Ston

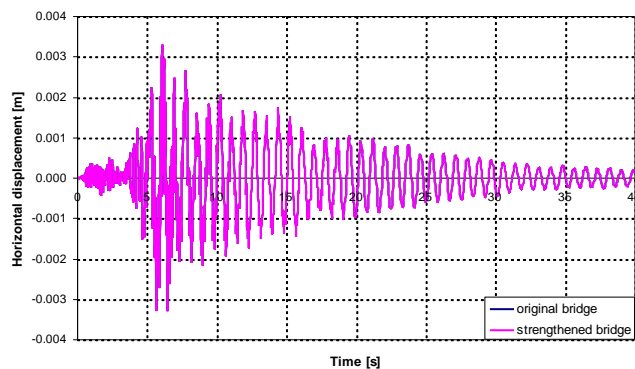


Fig. 27 Horizontal displacement of the top of a column for scaled earthquake Ston

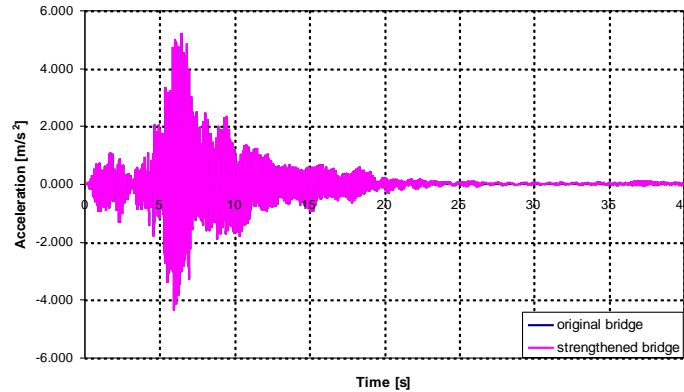


Fig. 28 Horizontal acceleration of the top of a column for scaled earthquake Ston

3.3 A composite concrete-steel bridge

A composite steel-concrete bridge near Split in Croatia (see Fig. 29) was analysed, as a part of its renovation project. However, steel girders are strengthened with new welded sheet $\neq 100/16$ mm at bottom flange. Strengthened bridge satisfies terms of bearing capacity and deformability according to existing Croatian norms HRN EN 1993-2:2008 and HRN EN 1994-2:2012. Both static and dynamic analyses for the original and strengthened bridge were performed. Scaled earthquake Ston with $PGA = 0.2$ g was used, which represents maximal design acceleration at the location of the bridge.

Deflection in the midspan of the bridge for gravitational and traffic loads is shown in Fig. 30.

The original bridge lost its stability at the traffic load factor of 1.45, while the strengthened bridge lost its stability at the traffic load factor of 1.9.

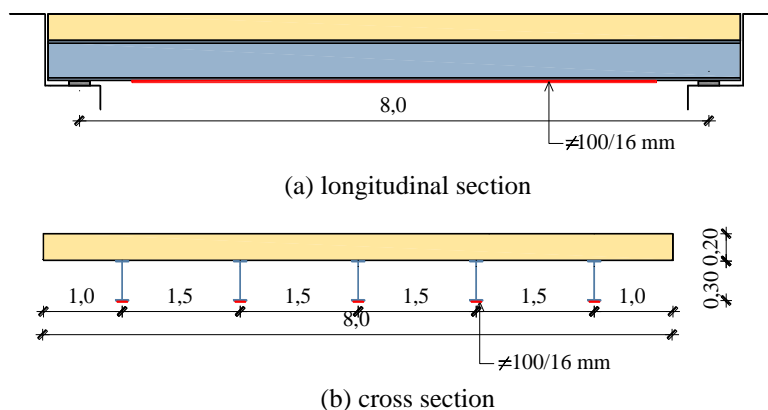


Fig. 29 Basic data of the analysed composite steel-concrete bridge

The strengthened bridge has increased stiffness (smaller displacements) than the original bridge for the equal traffic load.

Steel stress in the bottom flange in the midspan of the bridge for gravitational and traffic loads is presented in Fig. 31. For the equal traffic load, stresses in the strengthened bridge are greater than in the original bridge.

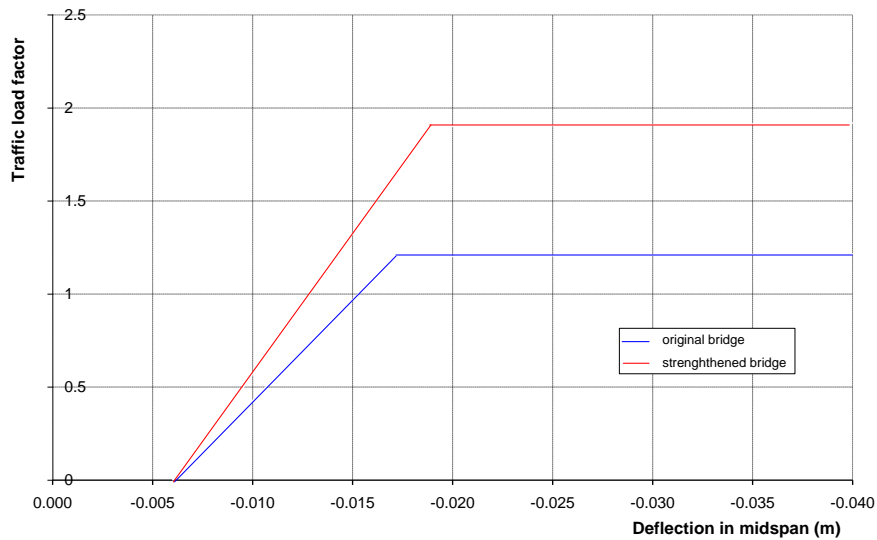


Fig. 30 Deflection in the midspan of the bridge for gravitational and traffic load

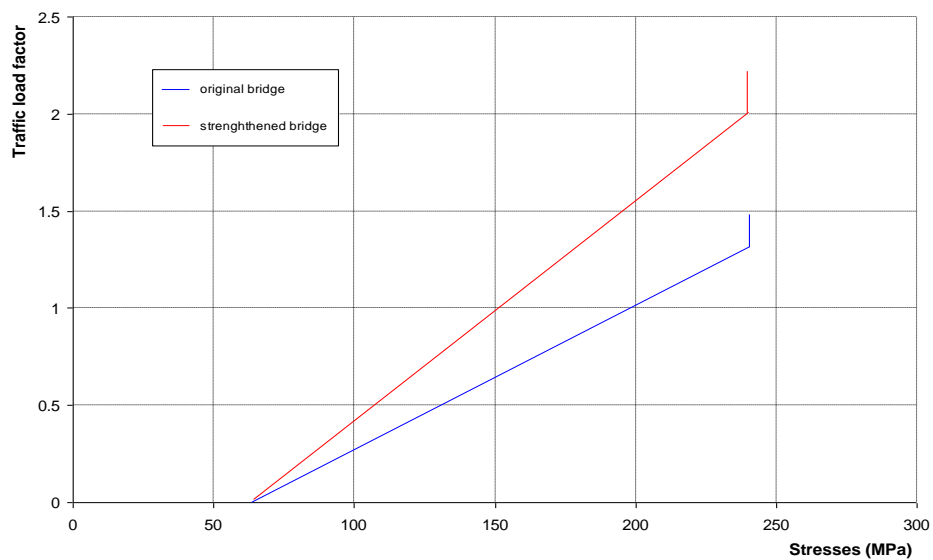


Fig. 31 Steel stress in the bottom flange in the midspan of the bridge for gravitational and traffic load

Stress in the new welded sheet in the midspan of the bridge for gravitational and traffic loads is shown in Fig. 32. For the scaled earthquake Ston, in combination with the dead load and 50% of the traffic load, deflection in the midspan is presented in Fig. 33, steel stress in the bottom flange in the midspan in Fig. 24 and stress in the new welded sheet in the midspan in Fig. 35.

Obtained results indicate that the strengthened bridge has greater bearing capacity and lower deflections compared to its previous state, in accordance with the requirements of Croatian norms HRN EN 1993-2:2008 and HRN EN 1994-2:2012.

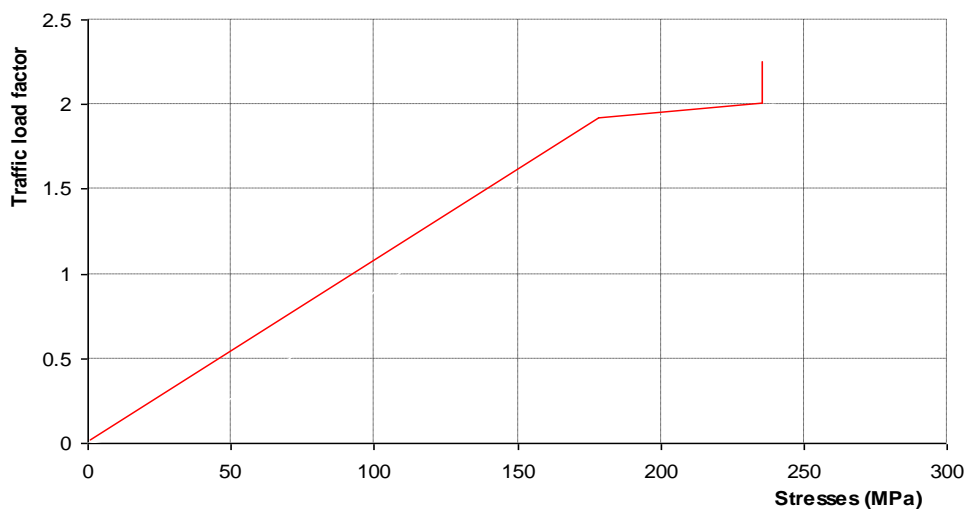


Fig. 32 Stress in the new welded sheet $\neq 100/16$ mm in the midspan of the bridge for gravitational and traffic load

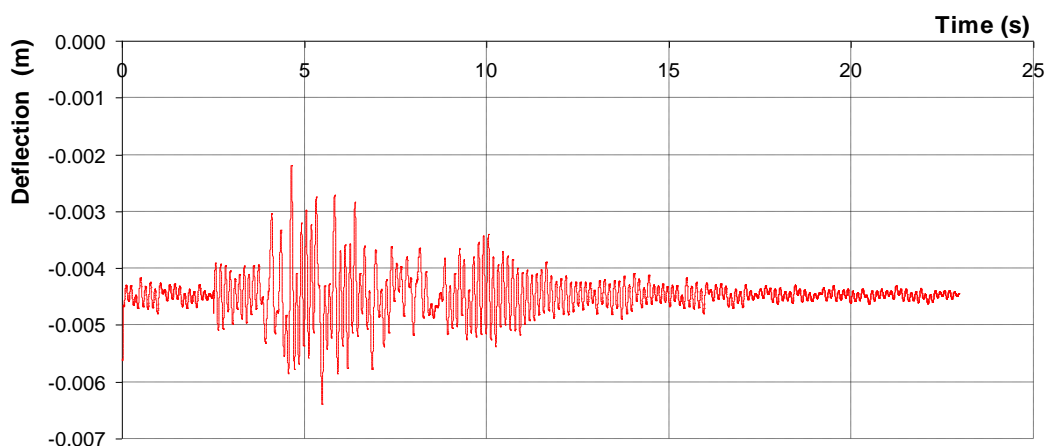


Fig. 33 Deflection in the midspan of the strengthened bridge for scaled earthquake Ston

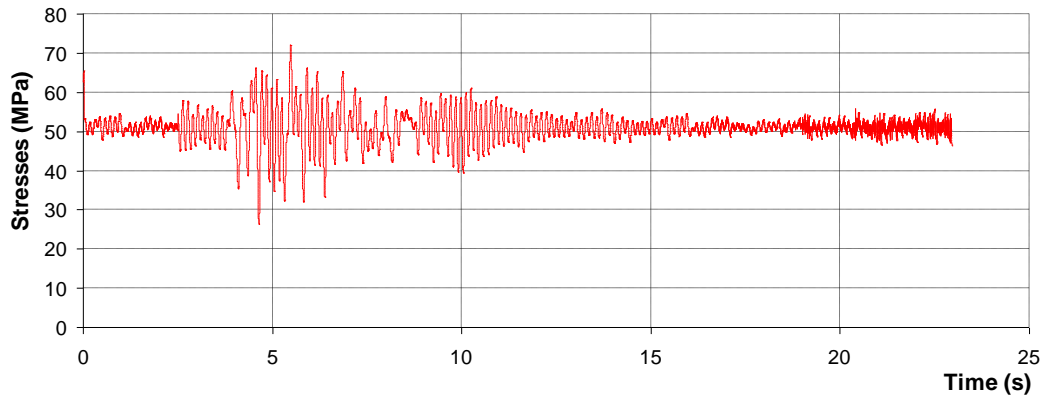


Fig. 34 Steel stress in the bottom flange in the midspan of the strengthened bridge for scaled earthquake Sten

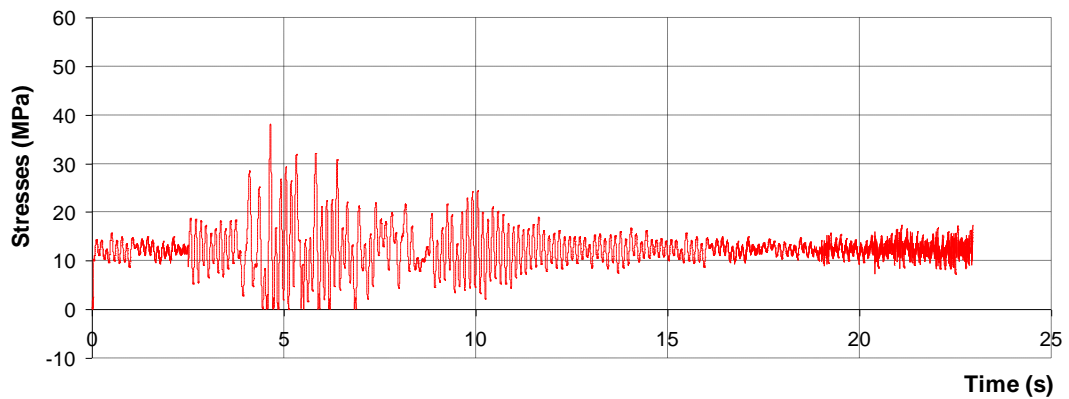


Fig. 35 Stress in the new welded sheet #100/16 mm in the midspan of the strengthened bridge for scaled earthquake Sten

4. Conclusions

Described numerical model and developed computer program 2D-COMPS for both static and dynamic analysis of individual and composite concrete-steel-masonry bridges can simulate their main nonlinear effects. The model is based on a small number of material parameters and can be useful in practical application. Analyzed examples show some possibilities of the developed numerical model. Future verifications of the presented model and corresponding computational software are most welcome.

Acknowledgments

This work was supported by the funds of the Ministry of Science, Education and Sport of Croatia. The authors appreciate their financial support.

References

- Abdessemed, M., Kenai, S., Bali, A. and Kibboua, A. (2011), "Dynamic analysis of a bridge repaired by CFRP: Experimental and numerical modelling", *Constr. Build. Mater.*, **25**(3), 1270-1276.
- Baloevic, G., Radnic, J. and Harapin, A. (2013), "Numerical dynamic tests of masonry-infilled RC frames", *Eng. Struct.*, **50**, 43-55.
- Berchio, E., Ferrero, A. and Gazzola, F. (2016), "Structural instability of nonlinear plates modelling suspension bridges: Mathematical answers to some long-standing questions", *Nonlinear Anal. Real World Applications*, **28**, 91-125.
- Brownjohn, J.M.W. and Xia, P.Q. (2000), "Dynamic assessment of curved cable-stayed bridge by model updating", *J. Struct. Eng. New York*, **126**(2), 252-260.
- Chung, W. and Sotelino, E.D. (2006), "Three-dimensional finite element modeling of composite girder bridges", *Eng. Struct.*, **28**(1), 63-71.
- Cunha, A., Caetano, E. and Delgado, R. (2001), "Dynamic tests on large cable-stayed bridge", *J. Bridge Eng.*, **6** (1), 54-62.
- Fu, C. (2016), "Dynamic behavior of a simply supported bridge with a switching crack subjected to seismic excitations and moving trains", *Eng. Struct.*, **110**, 59-69.
- HRN EN 1992-2:2013. Eurocode 2: Design of concrete structures -- Part 2: Concrete bridges -- Design and detailing rules.
- HRN EN 1993-2:2008. Eurocode 3: Design of steel structures -- Part 2: Steel bridges.
- HRN EN 1994-2:2012. Eurocode 4: Design of composite steel and concrete structures -- Part 2: General rules and rules for bridges.
- HRN EN 1998-2:2011. Eurocode 8: Design of structures for earthquake resistance -- Part 2: Bridges.
- Hughes, T.J.R., Pister, K.S. and Taylor, R.L. (1979), "Implicit-explicit finite elements in nonlinear transient analysis", *Comput. Method. Appl. M.*, **17-18**, 159-182.
- Krstevska, L., Kustura, M. and Tashkov, Lj. (2008), "Experimental dynamic testing of the Old Bridge in Mostar", *Proceedings of the International Scientific Symposium Modeling of Structures*, Mostar, Bosnia and Herzegovina, November.
- Li, Y., Cai, C.S., Liu, Y., Chen, Y. and Liu, J. (2016), "Dynamic analysis of a large span specially shaped hybrid girder bridge with concrete-filled steel tube arches", *Eng. Struct.*, **106**, 243-260.
- Radnic, J., Baloevic, G., Matesan, D. and Smilovic, M. (2013), "On a numerical model for static and dynamic analysis of in-plane masonry infilled steel frames", *Mater. Sci. Eng. Technol.*, **44**(5), 423-430.
- Radnic, J., Harapin, A., Matesan, D., Trogrlic, B., Smilovic, M., Grgic, N. and Baloevic, G. (2011), "Numerical model for analysis of masonry structure", *Gradjevinar*, **63**(6), 529-546.
- Radnic, J., Harapin, A., Smilovic, M., Grgic, N. and Glibic, M. (2012), "Static and dynamic analysis of the old stone bridge in Mostar", *Gradevinar*, **64**(8), 655-665.
- Song, M.K., Noh, H.C. and Choi, C.K. (2003), "A new three-dimensional finite element analysis model of high-speed train-bridge interactions", *Eng. Struct.*, **25**(13), 1611-1626.
- Wang, W., Deng, L. and Shao, X. (2016), "Number of stress cycles for fatigue design of simply-supported steel I-girder bridges considering the dynamic effect of vehicle loading", *Eng. Struct.*, **110**, 70-78.
- Yang, Y.B. and Yau, J.D. (1997), "Vehicle-bridge interaction element for dynamic analysis", *J. Struct. Eng.*, **123**(11), 1512-1518.